Universal scaling of fluid permeability for sphere packings

Nicos S. Martys,[1] S. Torquato,[2] and D. P. Bentz[1]

[1] *National Institute of Standards and Technology, Building Materials Division, Gaithersburg, Maryland 20899*

[2] *Princeton Materials Institute and Department of Civil Engineering and Operations Research, Princeton University, Princeton, New Jersey 08540-5211*

(Received 24 November 1993; revised manuscript received 18 March 1994)

Results from the numerical simulation of Stokes flow through random packings of nonoverlapping or overlapping spheres and a *scaling ansatz* are used to obtain universal curves for the fluid permeability. The scaling ansatz is motivated by previous analysis of rigorous bounds on the permeability. Excellent agreement was found for a variety of model microstructures of porous media in the low and high porosity regimes. Experimentally obtained permeabilities of several sandstones were found to agree well with our universal curve.

PACS number(s): 47.55.Mh

I. INTRODUCTION

The flow of fluids through random porous media plays an important role in a wide variety of environmental and technological processes; examples include the spread of hazardous waste in soils, the degradation of building materials such as concrete, the extraction of oil from porous rocks and separation processes such as chromatography [1,2]. The key parameter describing the macroscopic flow of a viscous fluid in a porous medium is the fluid permeability, k, defined by Darcy's law [3]

$$\mathbf{V} = -\frac{\mathbf{k}}{\eta}\frac{\mathbf{\Delta P}}{\mathbf{L}} \quad . \tag{1}$$

Here $\mathbf{V}$ is the average fluid velocity, η is the fluid's viscosity, and L is the length of the sample porous medium across which there is an applied pressure difference ΔP.

There has been a great deal of effort devoted to predicting fluid permeability based on knowledge of the porous medium's microstructure. Such calculations are difficult because the permeability depends on a large number of factors such as the porosity, typical pore size, connectivity of the pore space, and the tortuosity of the flow paths. Probably the most widely used empirical formula to predict permeabilty is the Kozeny-Carmen [3] relation

$$k = \phi_1^3/2s^2, \tag{2}$$

where ϕ_1 is the porosity and s is the specific surface (ratio of the pore surface area to the total volume of the sample). The rescaling of a porous medium by a factor of n will preserve its porosity but change the permeability by a factor n^2 (i.e., s decreases by a factor of n). Thus, an important role of the specific surface in the Kozeny-Carmen equation is to properly scale permeability data obtained from porous media described by different intrinsic length scales. It is also physically reasonable that increasing the surface area per unit volume, for a fixed porosity, should decrease the permeability since the fluid velocity must vanish along a surface. While the appeal of the Kozeny-Carmen relation is in part due to its simplicity, it breaks down in the high and low porosity regimes [4, 5]. Other more elaborate approaches to estimate or bound the permeability include the usage of cross-property relations based on pore space diffusion, electrical measurements and percolation ideas [6–8, 4, 9–11], and [5].

In this paper, we study the permeability of different classes of random three-dimensional porous media via direct numerical simulation of Stokes flow. A simple scaling ansatz, based upon previous analysis of rigorous bounds [10], is applied to the numerically determined fluid permeabilites. This scaling [which is a function of specific surface, volume fraction of solids ($\phi_2 = 1 - \phi_1$) and the critical porosity, ϕ_1^c, at which the pore space first percolates] causes the collapse of nearly all of the data onto a universal permeability curve. Results will be compared with other data obtained from experiment [12] and lattice gas [13] simulations of fluid flow in random porous media.

In Sec. II we describe the models of porous media and the method of fluid flow simulation. In Sec. III we discuss the scaling ansatz and show the collapsed data. We also deduce the functional form of the universal function. Section IV includes further discussion and our conclusions.

II. NUMERICAL SIMULATION: MODEL POROUS MEDIA AND STOKES FLOW

A. Model porous media

We simulate viscous flow through eight models of random porous media: models A–H. Except for model D, all porous media were constructed using periodic boundary conditions. Models A–D consist of various types of overlapping spheres, models E–G consist of different kinds of nonoverlapping-sphere packings, and H is a model of sintered porous media.

In model A, 500 monosized spheres of diameter 15 (in units of lattice spacing) were placed at random (without regard to overlap) on a 100^3 grid. The porosity was decreased by increasing the sphere diameters from 15.0 to 21.0 in steps of 2.0. In model B we again begin with randomly placed monosize overlapping spheres (diameter

15.0) in the 100^3 lattice, but the porosity is reduced by simply increasing the number of spheres from 500 to 1500. The third model, C, is constructed from different diameter spheres placed at random in a three-dimensional box of length 100. The sphere diameters were chosen from the values $\{3, 7, 11, 15\}$ with equal probability. The porosity for model C was varied by uniformly adding more spheres and the fluid flow equations were solved on the 100^3 grid. Model D is a sphere packing model used in Schwartz *et al.* [5] where spheres of three different diameters are dropped into a box and allowed to move about until a local equilibrium position is found. The radii of the spheres are $1, 10^{1/3}$, and $100^{1/3}$ and each sphere specified contributes equally to the total volume. The porosity is then varied by allowing the radii of the spheres to uniformly increase or decrease. An interesting feature of this porous medium is that as the spheres consolidate (increase in radius), the permeability becomes more anisotropic in contrast to the other pore models described in this paper which are inherently isotropic.

We also considered models of porous media composed of spheres which do not overlap. In model E, 10 000 spheres of diameter 5 are randomly placed in a 100^3 system. Here, $\phi_1 \approx 0.62$. In model F, 141 spheres each of diameters $\{3, 7, 11, 15\}$ were placed at random in a three-dimensional box of length 100. As in model E, $\phi_1 \approx 0.62$. We also simulate flow in a similar system with 173 spheres each from the same set of diameters but with $\phi_1 \approx 0.53$.

In model G the nonoverlapping-sphere system is generated using the Metropolis algorithm [14]. Spheres are initially placed in a cubical cell on the sites of a body-centered cubic lattice. The cell is surrounded by periodic images of itself. Each particle is then moved randomly (by some small amount) to a new position which is accepted or rejected according to whether or not hard cores overlap. *Periodic boundary conditions* are imposed (i.e., anytime a particle exits the face of the central cell its periodic image from a replicated cell enters the opposing face of the central cell) to simulate an infinite system (i.e., a statistically homogeneous medium). Equilibrium is achieved after moving each of the particles a sufficient number of times. This is checked by measuring the radial distribution function for the hard spheres at contact and comparing it to well-established values [14].

Model H is generated from simulations of reconstructed and sintered [15] porous media. The initial system (before being sintered) was actually a reconstruction of model A or B based on the autocorrelation [16] analysis of two-dimensional slices from these models. Once the three-dimensional image was created, a sintering algorithm [15], which in effect reduces the magnitude of local surface curvature gradients without changing the total porosity, was utilized to vary the specific surface until it matched the original sphere model's specific surface from which the two-dimensional slice was taken. A characteristic feature of this sintering model is that the pore space percolates at relatively high porosities. For the sintering model, $\phi_1^c \approx 0.09$ as compared to $\phi_1^c \approx 0.03$ for the overlapping sphere models.

Our study also includes data from lattice gas (LG) simulations of Stoke's flow due to Cancelliere *et al.* [13]. They determined the permeability of a system of randomly placed overlapping spheres of diameter 8 within a cube of volume 64^3. This model of porous media is similar to that of model B.

B. Numerical determination of fluid flow

In the limit of slow incompressible flow, steady state fluid flow is described by the linear Stokes equations

$$\eta \nabla^2 \mathbf{v}(\mathbf{r}) = \nabla p(\mathbf{r}), \tag{3a}$$

$$\nabla \cdot \mathbf{v}(\mathbf{r}) = 0, \tag{3b}$$

where $\mathbf{v}$ and p are, respectively, the local velocity and pressure fields, and η is the fluid viscosity. The fluid velocity must vanish at pore-solid interfaces and a pressure difference is applied at the inlet and outlet faces. To numerically solve the Stokes equations, we used a finite-difference scheme in conjunction with the artificial compressibility relaxation algorithm [4], [17], and [5]. The pore space is discretized into a marker-and-cell mesh [17], where pressures are defined at the nodes and fluid velocity components are defined along the center of bonds connecting nodes. Each voxel, a unit cube representing either pore or solid, is centered on a node. Near the pore-solid interface, noncentered difference equations are used to improve the accuracy of the solution and to force the fluid velocities to zero at the pore-solid interface. As a result, velocity profiles across voxels are accurate to at least second order [18]. In Fig. 1 we show a gray scale image of the fluid speed in Model A with $\phi_1 \approx 0.4$. The fluid speed has been thresholded so as to reveal more of the pattern of flow.

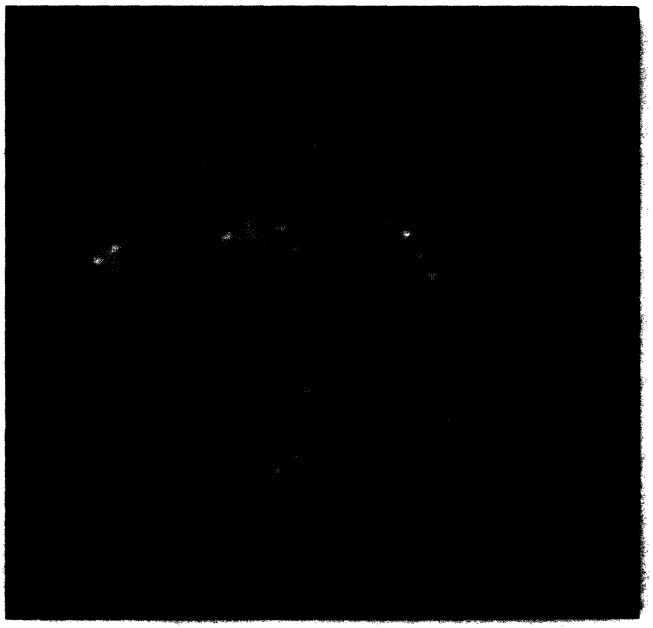

FIG. 1. Gray scale image of fluid flow in packed sphere model with $\phi \approx 0.4$. The spheres have been made transparent so that the flow pattern is easier to see. The lighter the image the greater the fluid speed.

The permeability of the porous medium is calculated by volume averaging the local fluid velocity and applying the Darcy equation (1). To account for fluctuations in permeability in the low porosity regime, we averaged the permeability of 8–10 realizations of each porosity investigated for models A and B to obtain a representative value. In addition, the average permeability of five samples for each porosity was determined for model H.

III. RESULTS

Figure 2 shows the unscaled permeability data as a function of porosity. The main factor contributing to the variation in permeability for a given porosity is the specific surface. However, at lower porosities fluctuations in the permeability increase as the critical porosity is approached. Figure 3 shows the standard deviation of permeability normalized to the mean value of permeability for models A, B, and H. At porosities greater than 0.3, the relative fluctuations are small. As the critical porosity is approached from above the relative fluctuations begin to diverge. Note also that Fig. 2 shows the anisotropy in permeability in model D. While the effect of anisotropy is small at the highest porosities, at very low porosities, such as $\phi_1 = 0.101$, the permeabiltiy varied up to a factor of 2.

We first consider a scaling scheme suggested by Torquato and Lu [10] to determine the universal behavior of an *upper bound* on the permeability derived by Doi [19]:

$$k_u = \frac{2}{3}\int_0^\infty r\left(F_{vv}(r) - \frac{2\phi_1}{s}F_{sv}(r) + \frac{\phi_1^2}{s^2}F_{ss}(r)\right)dr. \quad (4)$$

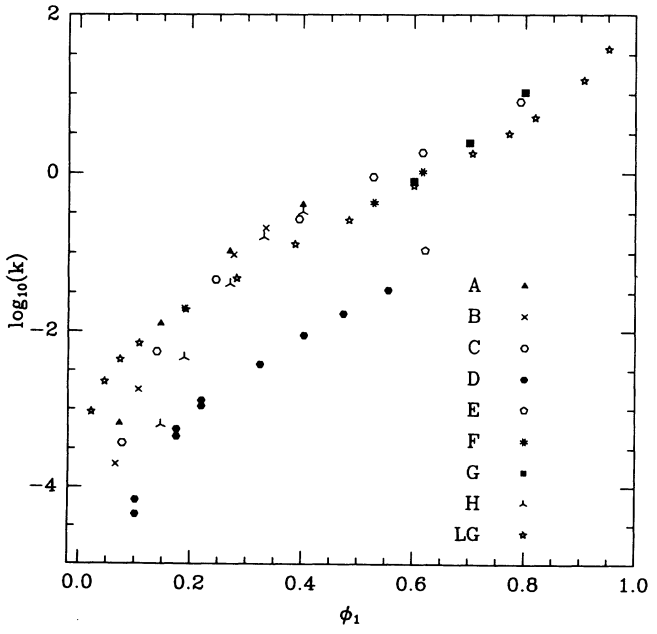

FIG. 2. The logarithm of the unscaled permeabilities for models described in text versus porosity.

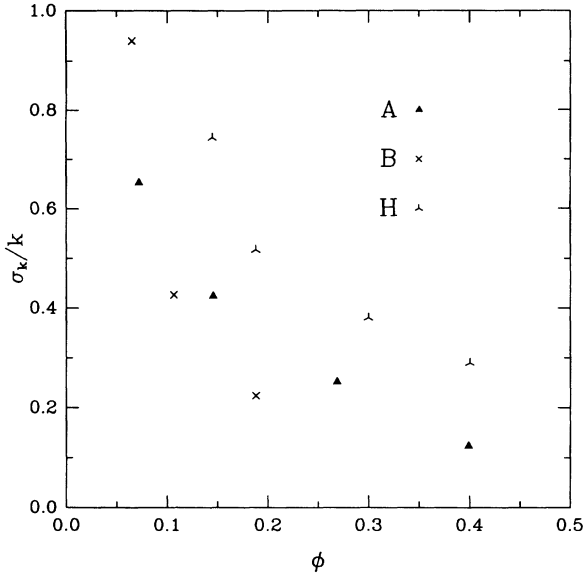

FIG. 3. The ratio of standard deviation of permeabilities to average permeability versus porosity. The relative fluctuation of permeabilities diverges as the critical porosity is approached.

The functions $F_{vv}(r)$, $F_{sv}(r)$, and $F_{ss}(r)$ are the void-void, surface-void, and surface-surface two-point correlation functions, respectively. Torquato and Lu evaluated this bound for porous media composed of overlapping spheres with a continuous size distribution. For a dilute bed of polydispersed spheres, the bound gives

$$k_o = 2\langle R^3\rangle^2/(9\langle R^2\rangle^2\phi_2). \quad (5)$$

Here $\langle R^n\rangle$ is the nth moment of the sphere size distribution. Torquato and Lu found that, to an excellent approximation, a universal curve for the upper bounds could be constructed by scaling k_u with k_o for each porosity.

In a similar manner, we rescaled our numerically determined permeabilities by k_o for the models A–D. Figure 4 shows that the rescaled data indeed collapses onto a universal curve.

One would like to be able to extend these scaling ideas to more complex microstructures (e.g., structure not constructed by spheres) in which determination of k_o may be more problematic. Toward this end, we note that for a dilute bed of polydispersed spheres k_o is simply equal to $2\phi_2/s^2$ [10], where ϕ_2 is the solid volume fraction and s is the specific surface. In Fig. 5 we scale the permeabilities of all of the models by $2\phi_2/s^2$ and find the remarkable result that for $\phi_1 > 0.3$ nearly all the data collapses onto a single curve. At lower porosities, the only data that does not collapse onto a single curve is that from the lattice gas (LG) simulations and the permeability data of flow through the sintered systems.

For porous media constructed by randomly overlapping spheres, as was used in the LG study and in all our simulations except for the sintered medium, the pore space should become disconnected at $\phi_1^c \approx 0.03$. While our simulation data is consistent with this value of ϕ_1^c,

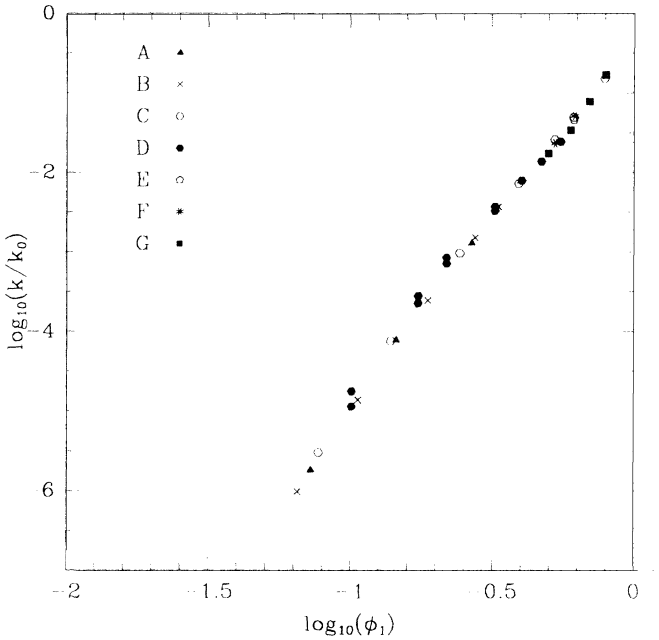

FIG. 4. The log of k/k_o vs log ϕ_1.

the LG simulation obtained relatively large values of permeability for $\phi_1 = 0.02$. We believe this nonzero permeability value to be a finite-size effect in their generation of the porous media. Accordingly, we will henceforth not consider the LG data in the low porosity regime.

In Figs. 2 and 5 permeability data from model H and a subset of data from models A and B can be compared. Note that systems with the same porosity also have matching s. We do not expect the permeability data from model H to overlap with results from models A and B in Fig. 5 because the sintering model has a higher $\phi_1^c \approx 0.09$ and, therefore, should produce considerably lower permeabilities at a given porosity and specific surface. In fact, at the lowest porosity tested, there was a factor of 20 difference in the permeabilities. To account for the difference in ϕ_1^c of these porous media models, we adjusted the porosity used in the scaling so that $\phi_1^* = \phi_1 - \phi_1^c$ (and $\phi_2^* = 1 - \phi_1^*$). We now find that all the data collapses onto a single curve.

Fitting data in the lower porosity regime, we found the following relation for permeability:

$$k = \frac{2\phi_2^*}{s^2}(\phi_1 - \phi_1^c)^f \quad , \tag{6}$$

where $f \approx 4.2$ (see Fig. 6). It is not clear whether we are close enough to the critical porosity to accurately determine f. However, it appears that this scaling is universal for a wide variety of porous media and is valid over many decades in permeability. The physical interpretation of Eq. (6) is that since $1/s$ is in general a length scale associated with a typical pore size, the power-law portion is accounting for the tortuosity and the connectedness of the pore space. The scaling in Eq. (6) is consistent with experiments [21] relating the permeability of glass bead packs, composed of a narrow distribution of bead diameters, with its conductivity. In these experiments $k \propto \sigma^2 \propto \phi^m$, where $m \approx 4$. We also point out that the permeability critical exponent we obtain is consistent with that obtained by Halperin *et al.* [20] for the "Swiss cheese" model, which is the same as model B.

Included in Fig. 6 is experimental permeability data obtained from a variety of natural sandstones due to Blair *et al.* [12]. Here we have taken $\phi_1^c = 0$ for the sandstone data where we are assuming that sandstone can be modeled as a packed aggregate. Again, there is reasonably good agreement between the experimental data and the universal curve.

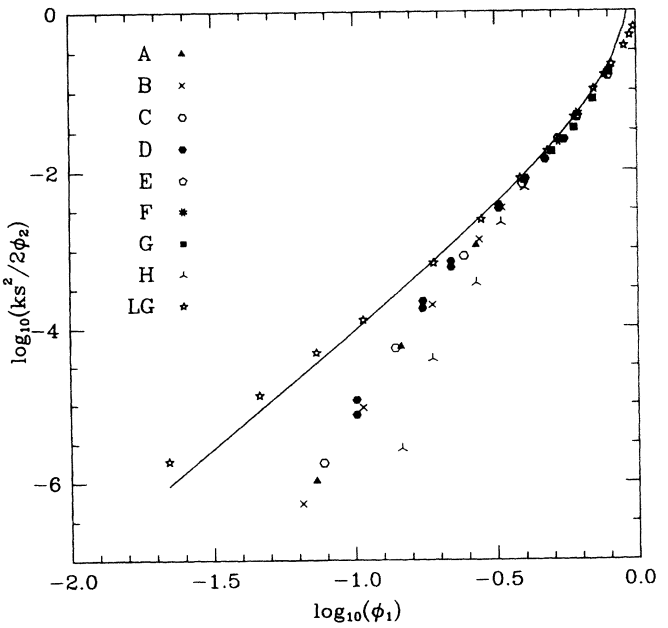

FIG. 5. The log of $ks^2/2\phi_2$ vs log ϕ_1. The solid line is the prediction of Kozeny-Carmen.

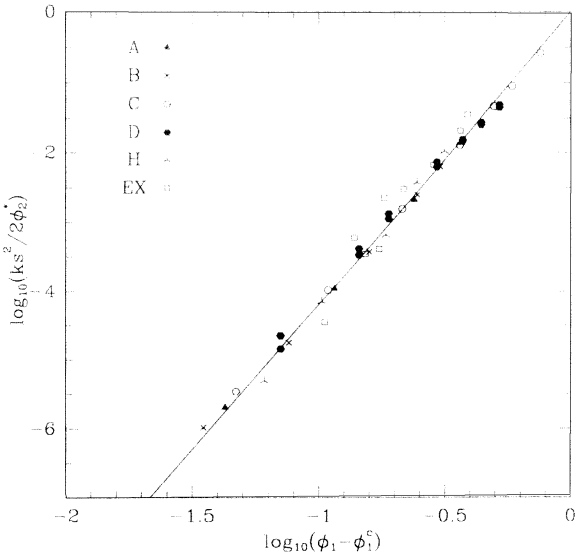

FIG. 6. The log of $ks/2\phi_2$ vs log of $\phi_1 - \phi_1^c$. The straight line corresponds to $f = 4.2$.

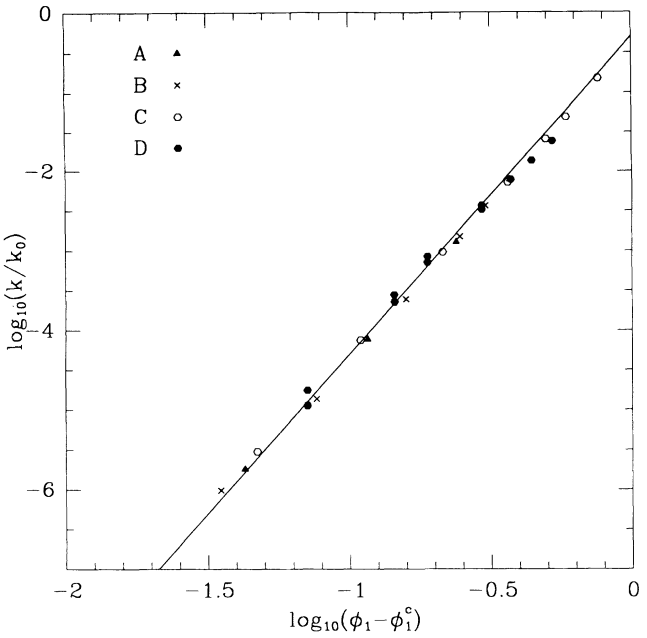

FIG. 7. The log of k/k_o vs log of $\phi_1 - \phi_1^c$. The straight line corresponds to $g = 4$.

Correcting the data scaled by k/k_o for the critical porosity as was done for the previous scaling by $2\phi_2/s^2$, we obtain the relation

$$k = k_o(\phi_1 - \phi_1^c)^g. \tag{7}$$

In this case, we find $g \approx 4$ (Fig. 7).

Why do both scaling ansatze produce *universal* curves (i.e., scaling permeability by $1/k_o$ or $s^2/2\phi_2$)? We found that for $0.5 < \phi_1 < 1$, there is only a 4% difference at most between the calculated values of $s^2/2\phi_2$ and $1/k_o$. As a result Figs. 4 and 5 should appear very similar. These scaling ansatze begin to differ more strongly as porosity is further decreased (by about 30% at the lowest porosites studied). Regardless, for the studied case of overlapping spheres, $1/k_o = f(\phi_1)s^2/2\phi_2$, where f is a function of ϕ_1 only, so that data will still collapse onto a single curve. While rescaling data with $s^2/2\phi_2$ or $1/k_o$ works very well, the former may be more useful in that it is much easier to determine s, whereas it is more difficult to relate k_o to more complex microstructures.

IV. SUMMARY AND CONCLUSIONS

In this paper, we have demonstrated the validity of a universal scaling ansatz for a variety of porous media and over a wide range of porosity. The utility of this scaling ansatz is that one need only know the specific surface, critical porosity and porosity of the material and then refer to the universal curves in Figs. 5 and 6 to obtain a reasonably good estimate of permeability. This scaling behavior is of course not expected for all realizations of porous media. For example, porous media with extremely convoluted (or rough surfaces) or large regions of disconnected space (voids) may not work as well since a considerable fraction of the pore space may not be dynamically connected to the main flow paths. At minimum, calculations of s would have to carefully take these regions into account. Moreover, as shown by Halperin *et al.* [20], there exist several universality classes of porous media (such as the inverted Swiss cheese model) where the scaling of permeability would not be the same as that in our study. A natural scaling parameter to try next is the aforementioned two-point bound $1/k_u$, since it is more general than $1/k_o$. Such scaling of permeability will be the subject of future studies. Further research is needed to improve our understanding of the scaling of permeability near the critical regime in other classes of porous media and to understand flow in highly anisotropic materials.

Finally, we note that for the class of porous media for which our scaling relations are valid, a measurement of the permeability k along with a knowledge of any pair of the triplet ϕ_1, s, ϕ_1^c can yield an estimate for the single unknown morphological parameter.

ACKNOWLEDGMENTS

We would like to thank Po-zen Wong for useful discussions. Work at Princeton was supported in part by the Petroleum Research Fund and the Office of Basic Energy Sciences, U.S. Department of Energy. Nicos S. Martys would like to thank Princeton University for financial support.

[1] Pierre M. Adler, *Porous Media: Geometry and Transports* (Butterworth-Heinemann, Boston, 1992), Chap. 7.
[2] Po-zen Wong, Phys. Today **41** (12), 24 (1988).
[3] A. E. Scheidegger, *The Physics of Flow Through Porous Media*, 2nd ed. (University of Toronto Press, Toronto, 1974).
[4] N. Martys and E. J. Garboczi, Phys. Rev. B **46**, 6080 (1992).
[5] L. M. Schwartz, N. Martys, D. P. Bentz, E. J. Garboczi, and S. Torquato, Phys. Rev. E **48**, 4584 (1993).
[6] A. J. Katz and A. H. Thompson, Phys. Rev. B **34**, 8179 (1986); J. Geophys. Res. **92**, 599 (1987).
[7] D. L. Johnson, L. M. Schwartz, and J. Koplik, Phys. Rev. Lett. **57**, 2564 (1986).
[8] J. R. Banavar and D. L. Johnson, Phys. Rev. B **35**, 7283 (1987).
[9] R. B. Saeger, L. E. Scriven, and H. T. Davis, Phys. Rev. A **44**, 5087 (1991).
[10] S. Torquato and B. Lu, Phys. Fluids A **2**, 487 (1990).
[11] M. Avellaneda and S. Torquato, Phys. Fluids A **3** (11), 2529 (1991).
[12] S. C. Blair, P. A. Berge, and J. G. Berryman, Lawerence Livermore National Laboratory, Report No. UCLR-LR-114182, 1993 (unpublished).
[13] A. Cancelliere, C. Chang, Enrico Foti, D. H. Rothman, and S. Succi, Phys. Fluids A **2**, 2085 (1990).

[14] See J. P. Hansen and I. R. McDonald, *Theory of Simple Liquids* (Academic Press, New York, 1986), and references therein.
[15] D. P. Bentz and N. Martys, Transp. Porous Media (to be published).
[16] J. A. Quiblier, J. Colloid Interface Sci. **98**, 84 (1984).
[17] R. Peyret and T. D. Taylor, *Computational Methods for Fluid Flow* (Springer-Verlag, New York, 1983).
[18] Suppose that, within a given voxel, we were to expand the exact solutions of the Stokes equations $\mathbf{v}(\mathbf{r}) \equiv \mathbf{v}(x, y, z,)$ as a Taylor series in x, y, and z. The use of noncentered difference equations guarantees that our solutions properly represent the first three terms of this expansion (i.e., that the errors are of order x^3 or x^2y, etc.).
[19] M. Doi, J. Phys. Soc. Jpn. **40**, 567 (1976).
[20] B. I. Halperin, S. Feng, and P. N. Sen, Phys. Rev. Lett. **54**, 2391 (1985).
[21] P. Wong, J. Koplik, and J. P. Tomanic, Phys. Rev. B **30**, 6606 (1984).

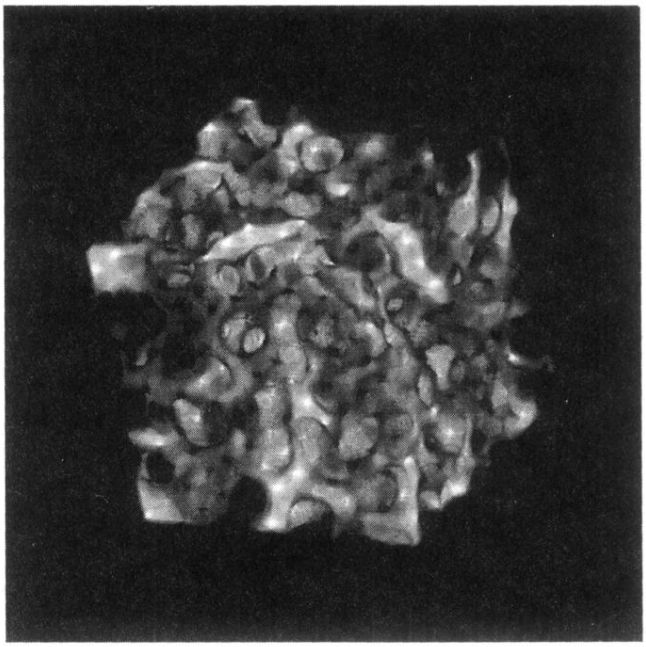

FIG. 1. Gray scale image of fluid flow in packed sphere model with $\phi \approx 0.4$. The spheres have been made transparent so that the flow pattern is easier to see. The lighter the image the greater the fluid speed.